ENVIRONMENTAL RESEARCH
COMMUNICATIONS

INCLUSIVE PUBLISHING
TRUSTED SCIENCE

Part of the
ENVIRONMENTAL RESEARCH
SERIES

PURPOSE-LED
PUBLISHING™

Glacier calving and moraine collapse triggered the glacial lake outburst flood in South Lhonak Lake, Indian Himalaya

To cite this article: Remya S N *et al* 2025 *Environ. Res. Commun.* **7** 115026

Environmental Research Communications

OPEN ACCESS

RECEIVED
20 March 2025

REVISED
25 July 2025

ACCEPTED FOR PUBLICATION
29 October 2025

PUBLISHED
26 November 2025

PAPER

Glacier calving and moraine collapse triggered the glacial lake outburst flood in South Lhonak Lake, Indian Himalaya

Remya S N[1,*], Vishnu Nandan[2,3], Atanu Bhattacharya[4,5], Pradeep Srinivasalu[6], Kriti Mukherjee[7], Babu Govindha Raj[8], John Yackel[3] and Tobias Bolch[9]

[1] School of Climate Change and Sustainability, Azim Premji University, Bengaluru, India
[2] Department of Electronics and Communication Engineering, Amrita Vishwa Vidyapeetham, Bengaluru Campus, Karnataka, India
[3] Department of Geography, University of Calgary, Alberta, Canada
[4] Department of Earth Sciences and Remote Sensing, JIS University, Kolkata, India
[5] Centre for Data Science, JIS Institute of Advanced Studies and Research, Kolkata, India
[6] Divecha Centre for Climate Change, Indian Institute of Science, Bengaluru, India
[7] Cranfield Environment Centre, Cranfield University, United Kingdom
[8] Indian Space Research Organization, ISRO Headquarters, Bengaluru, India
[9] Institute of Geodesy, Graz University of Technology, Austria
[*] Author to whom any correspondence should be addressed.

E-mail: remyannamboodiri@gmail.com

Keywords: Glacial lake outburst floods (GLOFs), Himalaya, calving, moraine, remote sensing, South Lhonak

Supplementary material for this article is available online

Abstract

Glacial lake outburst floods (GLOFs) are destructive and threaten downstream communities in the Himalaya. Through satellite image analysis, we investigate the 2023 GLOF event at South Lhonak Lake, Sikkim, India, focusing on the lake's historical evolution and the geomorphic controls that caused the GLOF. Multi-temporal data from 10 satellite missions revealed a significant increase in glacier surface lowering from -0.19 m year^{-1} (1970–1983) to -0.87 m year^{-1} (2015–2023). Initially a supraglacial lake in 1962, it evolved into a moraine-dammed lake by 1983 and expanded 12-fold from 0.11 km^2 (1962) to 1.4 km^2 (2023). Between 27 September and 6 October 2023, satellite imagery revealed an unusually strong retreat of 49.6 ± 7.1 m, indicating glacier calving and presence of massive icebergs visible on the lake. Our analysis shows 7 large glacier retreat and calving events between 2017 and 2023, further weakening the lateral moraines. This, combined with intermittent rainfall triggered the moraine dam collapse, leading to the GLOF. These findings emphasize the need for long-term monitoring of Himalayan glacial lakes.

1. Introduction

Shrinking glaciers contribute to sea-level rise, modify freshwater availability in mountain rivers and pose risks to the downstream community from glacier hazards (Zemp *et al* 2019, Immerzeel *et al* 2020). This includes ice avalanches, landslides and flood water from Glacier Lake Outburst Flood (GLOF) events (Emmer 2018), that can adversely affect more than 15 million people (Taylor *et al* 2023). GLOFs can be destructive leading to catastrophic damage to infrastructure, ecosystems, communities and loss of life. GLOFs originate from glacial lakes that store meltwater ahead of a retreating glacier, often behind a moraine dam formed by the accumulation of debris deposited by the glacier, or in exposed glacier beds where the topography is over-deepened (Carrivick and Tweed 2016). GLOF occurs if ice/moraine-dammed lakes fill and burst out suddenly, or if the confining moraine wall fails because debris mixed with ice is unable to contain the large volume of water and sediment (Harrison *et al* 2018). Recent shifts in climate patterns leading to accelerated snowmelt through warming and rain-on-snow events, calving of the glacier front adjacent to the lake, seismic activity, volcanic eruptions, and movement-induced impulse waves from avalanches caused by snow, ice and/or rocks

may all lead to GLOF events (Harrison *et al* 2018, Remya *et al* 2019, Ahmed *et al* 2021, Sattar *et al* 2021, Zheng *et al* 2021).

The Himalayan region is experiencing a growing likelihood risk from GLOF events (e.g. Allen *et al* 2022) and escalating frequency and intensity of GLOFs raise concerns about the vulnerability of the downstream community. Majority of the previous studies have primarily focused on evaluating glacier retreat associated with lake growth and GLOF potential (Raj *et al* 2013, Remya *et al* 2019, Sattar *et al* 2021). Other investigations (Staines and Carrivick 2015, Harrison *et al* 2018) have emphasized the importance of integrating observations and models to better understand glacial lake evolution and their physical processes such as climatological and geomorphic changes triggering GLOF events. However, rugged terrain, high altitudes and extreme climatic conditions pose significant challenges to *in situ* monitoring of GLOF-prone glacial lakes in Indian Himalaya. GLOFs can occur due to melting of buried ice under the moraine dam (Richardson and Reynolds 2000) and the thawing of ice and permafrost leading to ice/rock avalanches (Haeberli *et al* 2017, Harrison *et al* 2018), among others. Furthermore, research on modern GLOFs is hindered by the lack of detailed topographic data, which is essential for analysing the geomorphic changes that precede any GLOF event (e.g. Allen *et al* 2016). This limitation demands the need for localised investigations to accurately capture the processes that govern the triggers and timing of GLOF events.

Here, we focus on the GLOF event in South Lhonak Lake (SLL) in Sikkim Himalaya, India, that occurred on 4 October 2023. The flooding killed 178 people, left more than 70 people missing, destroyed homes and more than 30 bridges in several districts across Sikkim, and portions of Sikkim's biggest hydropower project (Zhang *et al* 2024). The likelihood for SLL burst out were forecasted earlier by Raj *et al* (2013), where they used optical remote sensing data from 1962–2008 and reported a 42% probability of SLL to outburst. Further, Remya *et al* (2019) studied SLL area and volume expansion and its vulnerabilities to outburst. After the SLL GLOF event occurred, studies by Kaushik *et al* (2024), Singh *et al* (2025), Yu *et al* (2024), Zhang *et al* (2024), Sattar *et al* (2025), and Saha *et al* (2025) used satellite-based remote sensing data, photogrammetric methods and dam breaching and hydrodynamic models to identify the triggers that led to the South Lhonak GLOF event. These studies concluded the collapse of the SLL's lateral moraine triggering multiple landslides as well as wave overtopping induced by landslide-generated impulse waves as the governing reasons for the GLOF. A detailed comparison between these studies and with our study is summarized in table T1 under Supporting Information .

Our study presents a comprehensive six-decade assessment (1962–2023) of the South Lhonak Glacier and SLL evolution, using high-resolution satellite stereo, optical and Synthetic Aperture Radar (SAR) imagery and DEM-based analysis. We quantify long-term mass loss and thinning trends of the glacier, and investigate changes in glacier retreat and frequency of calving events, historically and immediately preceding the GLOF event, and demonstrate increasing geomorphic instability of the lateral moraines over time. Complementing previous studies, our work goes further by examining the geomorphic evolution of SLL and conducting a historical multi-source satellite-based evaluation of elevation changes. Crucially, we assess the role of glacier calving and moraine instability in triggering the GLOF eventan aspect not addressed in earlier investigations. This approach allows for an in-depth understanding of the SLL dynamics, explaining how this GLOF occurred in response to geomorphic and glacial changes in the surrounding landforms.

2. Data and methods

2.1. Study area: South Lhonak Glacier and Lake

South Lhonak Lake is a proglacial lake originating from the South Lhonak Glacier (SLG) (27°54′18″ N and 88° 10′19″ E) (figure S1 in Supporting Information). The lake is located in the Teesta Basin, Sikkim Himalaya at an elevation of 5200 m above sea level (asl). To the north of SLG are the Lhonak Glacier and North Lhonak Glacier (NLG), which, together with SLG, comprise the 'Lhonak Glacier System'. The altitude of these three glaciers ranges from 5288 m asl to 7086 m asl. Adjoining the Lhonak Glacier is the Lhonak Lake, a proglacial lake formed by the glacier's retreat. There is a continuous flow of water from Lhonak lake and NLG into SLL via a narrow channel. The Teesta Valley, located near SLL, hosts numerous settlements and valuable assets along its river channel, particularly at Chungthang village, located about 71 km downstream from SLL.

2.2. Satellite and precipitation data

We used multi-sensor stereo optical imagery from 1962 to 2023 to map the evolution of SLL (table 1). For historical data, we processed different declassified high-resolution Corona KH-4 (spatial resolution 1.8 m–7.6 m) and Hexagon KH-9 panoramic camera stereo images (0.6 m–0.9 m). Elevation data for the period after 2000 were derived from SPOT-5 (5 m), ASTER-L1A (15 m), Cartosat-1 (2.5 m) and Pleiades-1A (0.5 m) stereo data. To assess lake morphology changes during the GLOF, we used imagery from PlanetScope (3 m), Sentinel-2A (10 m) and Sentinel-1 SAR (100 m). To quantify the frequency of glacier calving events, we used a

Table 1. Satellite and Rainfall datasets used in this study.

Parameter	Data Source	Spatial Resolution	Date/Period of Acquisition	Data Access/Reference
		Satellite Data		
Optical Reflectance and SAR Backscatter	Corona KH4A	2.75–7.5 m	15 Dec 1962	USGS Earth Explorer
	Corona KH4B	1.82–4.1 m	20 Nov 1970	
	Hexagon KH9 PC	0.6–0.9 m	11 Nov 1983	
	SPOT-5	5.0 m	1 Sep 2003	CNES SPOT World Heritage
	Cartosat-1	2.5 m	25 Nov 2009 and 9 Nov 2015	National remote Sensing centre (NRSC)
	Pleiades 1A	0.5 m	25 Oct 2022	https://dinamis.data-terra.org/en/eligible-users/
	ASTER L1A	15 m	7 Oct 2023	NASA EarthData
	PlanetScope	3.7 m	27 Sep 2023 and 6 Oct 2023	https://developers.planet.com/docs/data/planetscope/
	Sentinel-2A	10 m	Aug, Sep and Oct (2017–2023)	https://browser.dataspace.copernicus.eu/
	Sentinel-1 (SAR)	100 m	Aug, Sep and Oct (2017–2023)	https://browser.dataspace.copernicus.eu/
		Meteorological Data		
Daily rainfall	Global precipitation measurement	10 km	1 July 2023 -4 Oct 2023	https://gpm.nasa.gov/data/directory
Monthly rainfall	Global precipitation measurement		1 June 2000 - 31 Dec 2023	https://gpm.nasa.gov/data/directory
Daily rainfall	India Meteorological Department (IMD), Regional Meteorological Center (RMC), Kolkata	Lachen Weather Station (27.7°N, 88.5°E)	1 July 2023 - 4 Oct 2023	On request from IMD
Monthly rainfall	India Meteorological Department (IMD), Regional Meteorological Center (RMC), Kolkata	Chungthang Weather Station (27.6° N, 88.6°E)	Jan 2004 - Dec 2022	On request from IMD

combination of cloud-free imagery from Sentinel-2A and Sentinel-1 SAR from 2017 to 2023. We also examined the impact of precipitation on GLOF events at daily and monthly scales using Global Precipitation Measurement (GPM) data at 10 km resolution, along with rainfall data from the Indian Meteorological Department's Lachen and Chungthang weather stations (table 1).

2.3. Estimating glacier elevation changes from 1962–2023

We generated DEMs from the declassified Corona-KH4 using modified collinearity equation-based image distortion model (Sohn *et al* 2004) available with the Remote Sensing Software Package Graz. We automatically identified tie points using Förstner operator (Förstner and Gülch 1987) to coregister the stereo pairs. To reduce the parallax errors of Corona-KH4 panoramic camera image strips, we applied a polynomial rectification. Finally, disparity predictions were matched using various search windows in both directions (Goerlich *et al* 2017).

We used the Corona Stereo Pipeline (CoSP) workflow (Ghuffar *et al* 2023) to generate DEMs from KH9 Panoramic Camera images. DEMs from the rest of the stereo pairs (ASTER-1A, SPOT-5, Cartosat-1 and Pleiades 1A) were generated by AMES Stereo Pipeline (ASP, v3.1.0) developed by the National Aeronautics and Space Administration (NASA). We used a rational polynomial coefficient (RPC) model for stereo triangulation and Semi Global Matching (SGM) correlation algorithm to generate the DEMs.

Different DEM pairs were co-registered with each other following Nuth and Kääb (2011). After co-registration, pixels showing elevation changes outside ± 150 m were removed. Next, a three-cell buffer was applied around data gaps to eliminate high-magnitude elevation differences (Falaschi *et al* 2023). We also used an elevation-dependent sigmoid function to remove outliers from low contrast declassified Corona KH4 and Hexagon KH9 data (Pieczonka and Bolch 2015). Continuous elevation change grids were generated by filling data gaps in DEM difference images, using the global mean hypsometric approach (McNabb *et al* 2019), fitting a third-order polynomial to mean elevation changes across 50 m elevation bins. The overall glacier mass balance uncertainty was assessed by considering uncertainties in (1) surface elevation change following Fischer *et al* (2015), (2) glacier volume uncertainty (Brun *et al* 2017) by using fraction of valid data point, error (10%) in estimating initial glacier area and mean rate of elevation change in the glacierized area, and finally (3) volume-to-mass conversion factor (800 kg m^{-3}) and the uncertainty of the volume-to-mass conversion factor (60 kg m^{-3}) following Huss (2013). The SLL glacier retreat between 1962 and 2023 is calculated along the glacier's central flow line following Bhambri *et al* (2012). The uncertainty of the terminus changes from the optical imagery used in this study is calculated following Hall *et al* (2003) given by $U_T = \sqrt{a^2 + b^2} + \sigma$, where U_T is the uncertainty and a and bf are the pixel resolution (in meters). The glacier area uncertainty is estimated following the buffer method described in Bolch *et al* (2010) and Granshaw and Fountain (2006). The uncertainty of lake area is estimated by Basnett *et al* (2013), given by $a = NA/2$, where N is the number of pixels around the lake boundary and A is the pixel area.

2.4. Quantifying pre- and post-GLOF changes on the lake and glacier calving events

We used Sentinel-2A and Sentinel-1 SAR imagery from 25 September and 7 October 2023 to identify changes in the SLL pre- and post-GLOF event. We also collected Sentinel-1 SAR backscatter imagery of SLG during the summer months of August, September and October between 2017 and 2023. This was to quantify the frequency of glacier calving events to assess its impact on the lateral moraines and the SLL volume and mass balance. When at least 20% of the SLL area was covered with calved ice bergs, we record it as a calving event. Winter months were omitted to avoid confusion between calved ice from the SLG versus SLL ice break up events.

2.5. Identifying moraines and permafrost surrounding the lake

This analysis included characterization of moraine evolution, characteristics of both NLG and SLG, and potential presence of permafrost surrounding SLL. Moraine evolution from 1962 to 2023 is categorized using the DEMs from high resolution satellite data, based on their characteristic shape and location relative to the glacier (e.g. Zhang *et al* 2022). We delineated the lateral and terminal moraines, identified based on their distinctive visual characteristics in the imagery (figure S2 in Supporting Information). For example, lateral moraines are ridges of debris deposited along the sides of a glacier, marking the maximum lateral extent of past glacier advance (e.g. Remya *et al* 2024). Terminal moraines are ridges of debris deposited at the snout or end of a glacier, indicating the glacier's past extent and its retreat or advance history. Proglacial lakes are formed in front of a glacier, typically dammed by moraines or ice, with their extent and position providing information on past glacier margins (Raj *et al* 2013). By comparing the digitized boundaries and identified features across different epochs, we assessed changes in the lake's size, shape, and surrounding geomorphology. This included calculating glacier area changes and observing changes in moraines. To understand the dynamic nature of the North Lhonak and Lhonak glaciers in relation to the SLL, we explore their distinct flow patterns and terminus

positions between 1962 and 2023. The determination of the probable spatial distribution of permafrost has been considered as one of the fundamental components of mountain hazard and risk assessment studies (e.g. Allen *et al* 2016). We use the Permafrost Probability Fraction following Obu *et al* (2019) and Permafrost Zonation Map following Gruber (2012), both at 1 km^2 spatial resolution to map the distribution of permafrost around the SLL. The data from Obu *et al* (2019) is between the 2000–2016 period, while the Gruber (2012) dataset covers between 1961 and 1990. We use these datasets only to show the past and present occurrence of permafrost in the study region.

2.6. Analysis of rainfall data

There is no meteorological station located close to SLG. The nearest station from where daily rainfall data for the period 1 July to 4 October 2023 was available is Lachen Station (27.7° N, 88.5° E; 2710 m asl), located ∼40 km south-east of SLL. Additionally, long term monthly rainfall observations from 2004–2022 was available for Chungthang Station (27.6° N, 88.6° E; 1770 m asl), approximately 55 km south-east to the lake. In absence of meteorological stations closer to the glacier, we use rainfall data from NASA Global Precipitation Measurement (GPM) known as Integrated Multi satellitE Retrievals for GPM (IMERG) final run daily rainfall products for the grid representing the glacier. To understand how well GPM data agrees with the station observations, we also extracted the GPM data of the nearest grids from the station locations. This data is available at 10 km spatial resolution and is generated by calibrating, merging and interpolating satellite precipitation estimates with precipitation gauge analysis and other precipitation estimators over the globe (Huffman *et al* 2020), and hence is expected to best approximate the ground truth. We utilize the research-grade final run GPM product (v07), that incorporates data from the Tropical Rainfall Measuring Mission (TRMM) spanning June 2000 to April 2015, and the GPM dataset covering the period from April 2015 to present.

3. Results

3.1. GLOF characteristics and glacial calving events

Our analysis of PlanetScope and Sentinel-1 SAR imagery from before and after the GLOF event on 27 September and 6 October 2023, respectively, revealed significant glacier retreat and changes in SLL (figures 1(a) to (f)). The glacier retreated by 49.6 ± 7.1 m over these 10 days. The post-event imagery from 6 and 7 October (figure 1(d)) also indicated the presence of floating ice mass on the lake, caused by the calving of the glacier front. The lake area was reduced from ∼170 hectares on 27 September to ∼150 hectares on 7 October. The lake appears to extend toward the northern lateral moraine adjacent to the glacier, suggesting the collapse of the moraine wall, consistent with observations from Zhang *et al* (2024). The rapid detachment of a large ice mass would have displaced significant volumes of water, causing an overflow of the moraine dam. The existing outlet of the SLL has subsequently been eroded and widened. The extension of the lake toward the northern lateral moraine and the collapse of this moraine could likely be directly tied to a calving event. The moraine, previously supported by the glacier ice, may have become destabilized as the glacier retreated and calved, resulting in its collapse due to debuttressing.

Analysis of Sentinel-1 SAR time series indicates 7 major SLG calving events that occurred during the summer months between August and October from 2017 to 2023, including the calving event that caused the 2023 GLOF. As an example, we show the calving event from 24 and 27 October 2022, as seen from Sentinel-1 SAR and Sentinel-2 optical imagery (figures S2(a), (b), (d), (e)) in Supporting Information). Calved ice bergs were found to cover more than 50% of the lake area and likely stabilized the SLG through buttressing until 9 June 2023 (as observed from Sentinel-2) after which the calved ice melted off (figures S2(c) and (f) in Supporting Information).

3.2. Decadal changes in glacier retreat, elevation and lake evolution

From 1962 and 1970 imagery, the SLL was supraglacial with an area of 0.113 ± 0.006 km^2 and 0.165 ± 0.002 km^2 (figures 2(a) and S3 in Supporting Information). In the 1983 image, SLL evolved into a moraine-dammed lake with an area of 0.321 ± 0.002 km^2. By 2003, SLL expanded to 0.765 ± 0.01 km^2 and to 1.4 ± 0.011 km^2 by 2023: almost a 12-fold increase since 1962 and nearly double its size between 2003 and 2023. The lake volume followed a similar trend, tripling from 19.50 ± 3.51 million m^3 in 2003 to 73.79 ± 13.28 million m^3 in 2023 (figure 2(a)). The average depth of SLL also doubled from 25.64 ± 3.33 m in 2003 to 50.48 ± 6.56 m in 2023 (figure 2(a)). This accelerated glacier retreat post 1983 played a key role in the rapid enlargement of SLL. SLG experienced a steady retreat with its highest retreat rate between 1962 and 1970 (figures 2(b), (d)), when it formed a supraglacial lake, retreating by 660.8 ± 29.35 m during this period, with an average rate of 86.6 ± 3.85 m $year^{-1}$. The retreat rate then slowed to 20 ± 0.89 m $year^{-1}$ from 1970 to 1983, which is the minimum

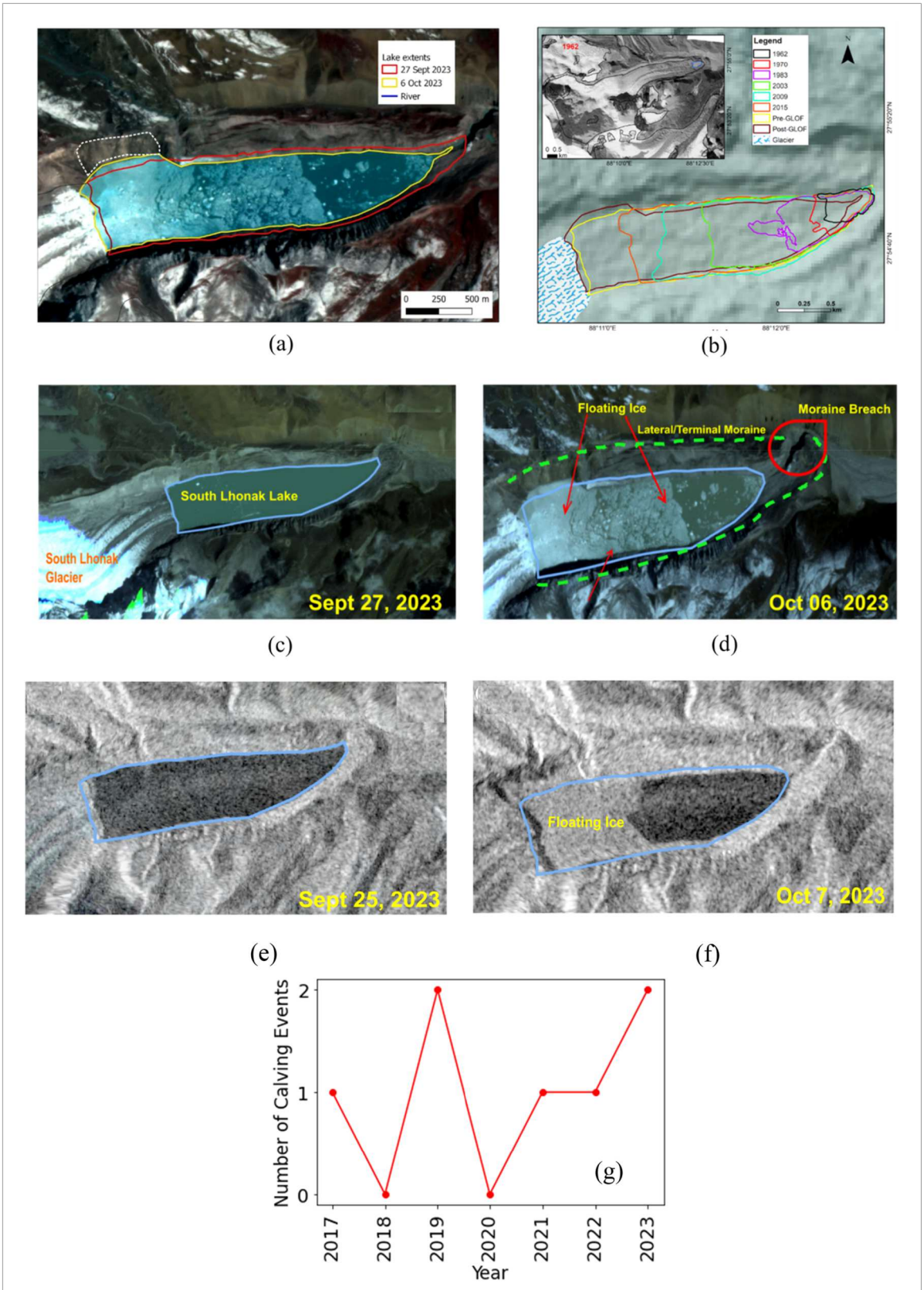

Figure 1. (a) PlanetScope imagery of SLL showing change in lake and glacier terminus from 27 September to 6 October 2023. Dotted white line indicates the region where the moraine wall collapsed; (b) area evolution of the lake using high resolution data from 1962 to 2023; (c) SLL and SLG before the GLOF event on 27 September 2023 as seen from PlanetScope optical imagery; (d) SLL after the GLOF event on 6 October 2023 with floating ice and debris as seen from PlanetScope optical imagery; (e) SLL before the GLOF event on 25 September 2023 as seen from Sentinel-1 SAR backscatter imagery; (f) SLL after the GLOF event on 7 October 2023 with floating ice as observed from Sentinel-1 SAR; and (g) Number of calving events as recorded from Sentinel-1 SAR between the months of August to October from 2017 to 2023. Note: The blue polygon in panels (c) to (f) show the approximate extent of SLL before and after the GLOF. (Optical and SAR image copyright: Planet Labs and ESA Copernicus (2023)).

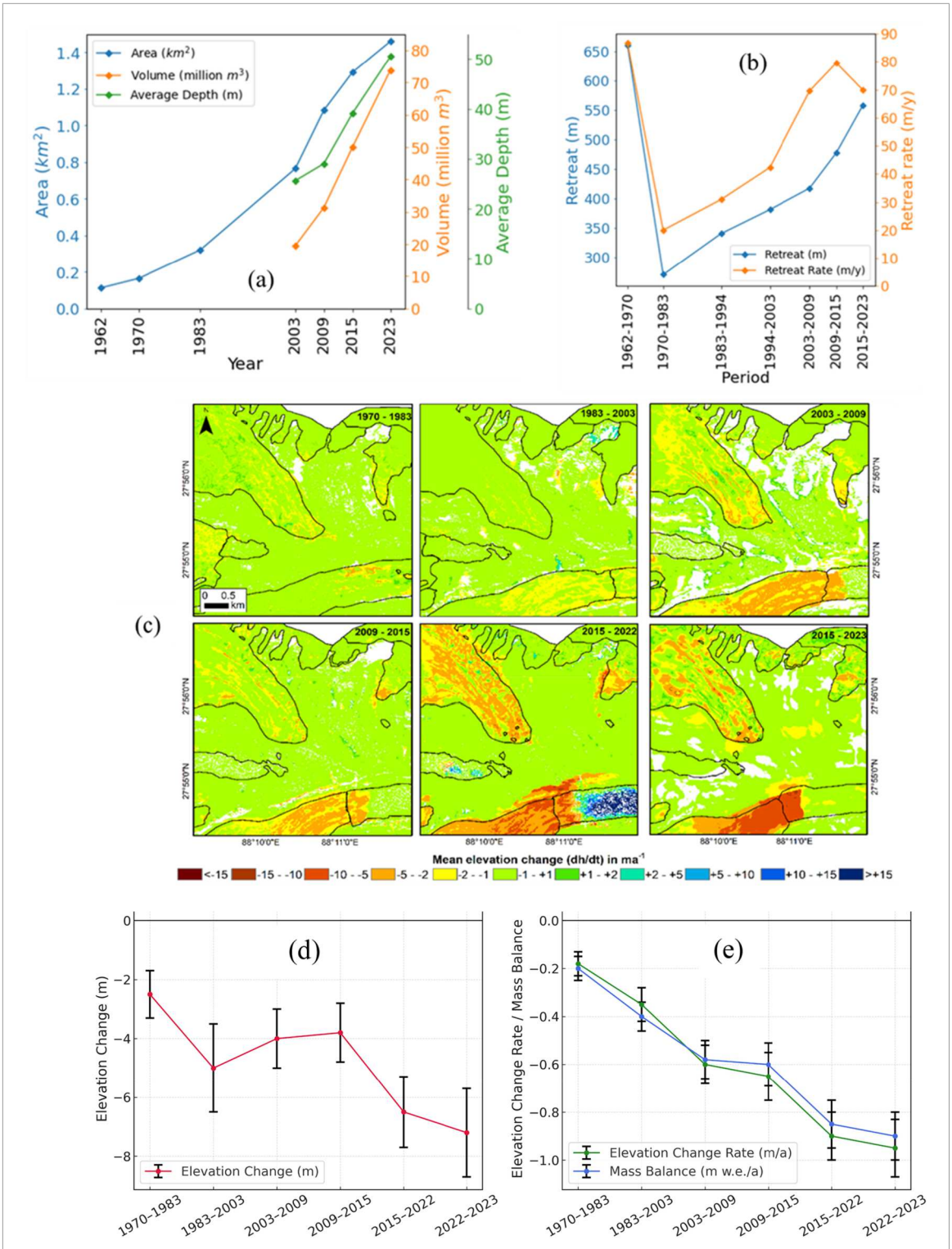

Figure 2. (a) Area change (1962–2023), volume change (2003–2023) and average depth of the lake change (2003–2023), (b) Retreat distance (1962–2023) and rate of retreat of the glacier between 1962 and 2023, (c) Surface elevation change rate (m/a), showing the spatial distribution around SLG, highlighting glacier retreat and lake expansion over time, (d) temporal elevation change trends observed for various time intervals from 1970 to 2023, and (e) mass balance and elevation change rate, from 1970 to 2023.

retreat rate compared to any previously recorded period. From 1983 to 2023, the retreat rate increased once more, contributing to the expansion of the SLL (figure 2(c)).

To analyze the elevation changes in the landforms nearby SLL, we have analysed decadal elevation change using the DEMs. We observed an increasing trend of elevation loss from 1970 to 2023 (figure 2(d)). SLG has undergone substantial thinning since 2003. The rate of ice loss increased from -0.19 ± 0.06 m year^{-1} before 1983 to -0.67 ± 0.11 m year^{-1}/a between 2003 and 2009. The loss rate slowed (-0.65 ± 0.11 m year^{-1}) slightly after 2009, but again increased to -0.90 ± 0.13 m year^{-1} in the most recent period (2015–2022) (figure 2(d)).

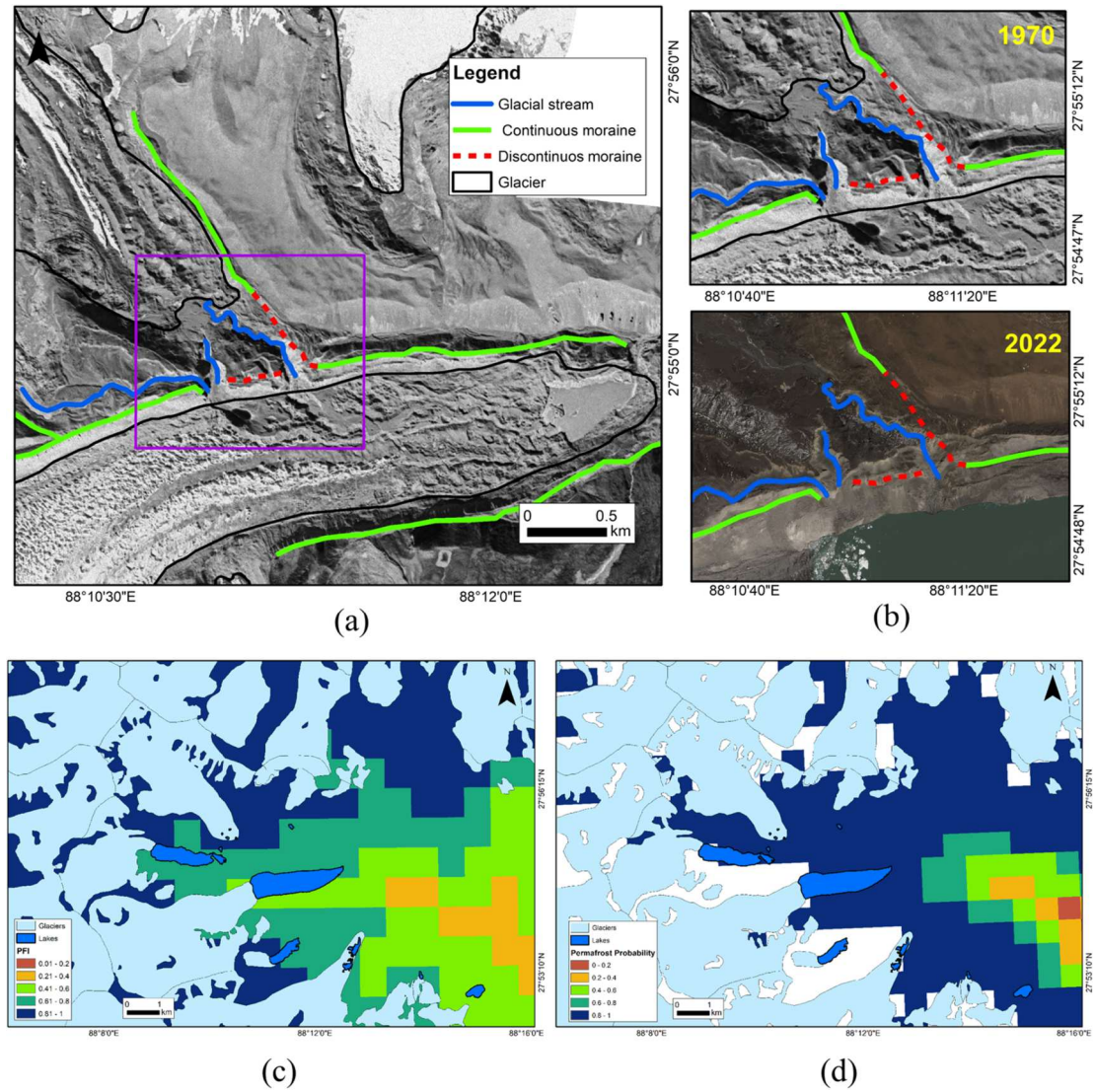

Figure 3. (a) Historical (1970 image) moraine distribution and other glacial landforms near SLL, (b) Lateral moraine evolution and its comparison between 1970 and 2022, (c) Permafrost Zonation Index Map (PZM) from 1961 and 1990 following Gruber (2012), and (d) Permafrost Probability map following Obu *et al* (2019), illustrating permafrost distribution near SLL and its surrounding area from 2000 to 2016.

During 2015 to 2023, the rate of elevation loss decreased slightly to -0.87 ± 0.19 m year^{-1} (-0.74 ± 0.16 m w.e.year^{-1}). However, considering the uncertainty limit, the difference is not significant (figure 2(e)).

3.3. Moraine evolution and permafrost occurrence

Continuous lateral moraines are clearly visible on both sides of the SLG in the 1970 image (figure 3(a)). At the same time, the north lateral moraine shows discontinuity, with a stream from the Lhonak glacier flowing down and breaking through the lateral moraine (figure 3). At that time, SLL had not developed into a moraine-dammed lake, and this stream continued downstream through the lateral moraine wall of the glacier. In contrast, the 2022 image reveals that this stream now contributes to the SLL, flowing through the lateral moraine (figure 3(b)). This configuration rendered the north lateral moraine potentially unstable. Additionally, another discontinuous lateral moraine originating from Lhonak Glacier is joining with the discontinuous lateral moraine of SLG indicating Lhonak Glacier was a tributary glacier to the South Lhonak trunk glacier during the peak of glaciation (figure S4 in Supporting Information). The Lhonak Glacier recession resulted in separation of the two glaciers. When Lhonak Glacier was actively contributing to SLG as a tributary, their lateral moraines formed a continuous depositional system. Upon the retreat of the Lhonak Glacier, its terminal moraine, rich in ice-mantled debris, was deposited and subsequently integrated into the lateral moraine of the SLG. This has led to a segmented structure in the SLG's lateral moraine, as the former terminal moraine of the Lhonak Glacier no longer aligns with the continuous lateral morphology of SLG. This disjointed configuration contributes to the moraine's overall instability, a characteristic visible in recent satellite imagery. In Himalayan

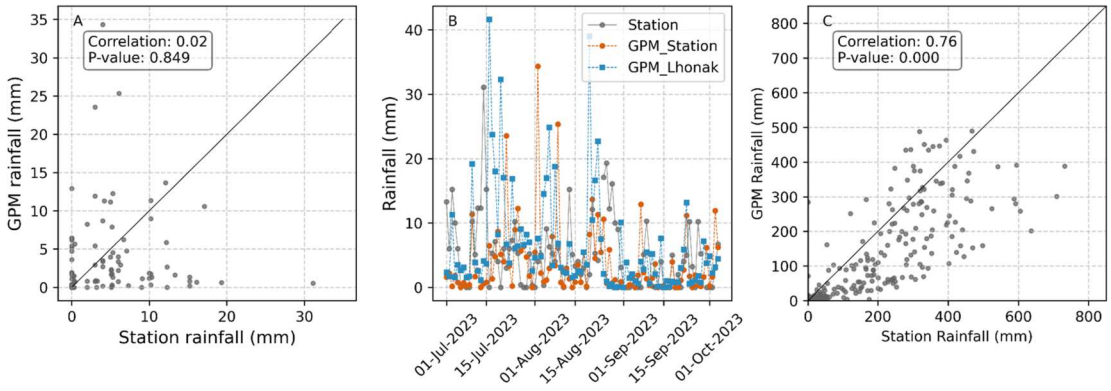

Figure 4. (a) Daily Station (Lachen) versus GPM rainfall observations; (b) Time series of daily rainfall observations; (c) Monthly rainfall observations from Chungthang Station compared against GPM observations.

glaciers, terminal moraines are typically ice-cored, making them more prone to breakage and collapse compared to the more stable lateral moraines (Raj *et al* 2013). The derived-products from Gruber (2012) and Obu *et al* (2019) around the North and South Lhonak lakes confirms the presence of permafrost (figures 3(c), (d)). High probabilities are also observed in elevated areas extending north of the lake towards the mountainous terrain, where the presence of permafrost is suspected based on the PMZ.

3.4. Quantifying rainfall characteristics during GLOF

We observed no correlation between the daily Lachen station data and the corresponding GPM grid observations (figure 4(a)). While both datasets record a maximum daily rainfall of approximately 35 mm during July-August 2023, the specific days on which these events occur differ between the two (figure 4(b)). From 1 September until the event on 4 October, both datasets show a maximum daily rainfall of around 10 mm. Overlaying with the daily GPM data of the glacier location indicates similar rainfall patterns, with maximum daily rainfall of around 40 mm observed between 1 July and 31 August 2023. The magnitude decreases thereafter, with a maximum daily rainfall of ∼15 mm in September. For the monthly rainfall data we observe that there is a high statistically significant positive correlation ($r = 0.76$, $p < 0.01$) between the GPM and corresponding station observations. However, we also observe that the station rainfall values are often significantly higher than the values represented by the GPM grid (figure 4(c)).

4. Discussion

4.1. Six decades of geomorphic and elevation change around the glacial lake

Our results indicate a substantial increase in the SLL area, from 0.1 km^2 in 1962 to 1.5 km^2 in 2023, highlighting significant glacial retreat and melting over this period. Glacier elevation changes reveal increasingly negative trends, from -0.19 m $year^{-1}$ in 1973 to -0.87 m $year^{-1}$ in 2023, indicating accelerated thinning and mass loss of SG. These results align with Remya *et al* (2019), who reported the lake area grew between 0.80 km^2 and 1.30 km^2 from 2001 to 2015, additionally with a modelled lake volume of 60 million m^3 and a maximum depth of 170 m during 2015. In contrast, Raj *et al* (2013) observed a comparatively smaller expansion of 0.811 km^2 from 1977 to 2008. The discrepancy may be attributed to differences in the temporal resolution and datasets used by Raj *et al* (2013), where they utilized MSS data from 1977 (90 m), which has a lower spatial resolution, and Remya *et al* (2019) used Landsat imagery (15 to 30 m), while our study uses higher resolution from Corona and PlanetScope. Additionally, our observations of glacier calving from Sentinel-1 SAR imagery due to rapid glacier retreat before the GLOF event and also since 2017 aligns with observations from Sharma *et al* (2018), where they reported significant glacier calving and the presence of ice masses in SLL. Presence of ice masses on the lake would have likely destabilized and de-buttressed the surrounding moraine walls, triggering large amounts of sediment transport into the lake (Zhang *et al* 2024).

4.2. GLOF preconditioning and triggering factors

4.2.1. Glacier calving

Analysis of pre- and post-GLOF images revealed that there was a substantial retreat (49.6 ± 7.7 m) of SLG front between 27 September and 6 October 2023. Such retreat was not observed in any of the neighboring glaciers over the same period. Sentinel-1 SAR observations of the SLL during the GLOF event and since 2017 during the

summer months shows substantial glacial calving (n = 7 between 2017 and 2023). Our findings are validated by field observations from the SLL by Sharma *et al* (2018), where they documented substantial ice calving during the summer melting season. Given the history of glacier calving as a trigger for dynamic changes in SLL, the detachment of ice masses from the glacier terminus can generate substantial wave activity within the lake. These waves exert significant pressure on the lateral moraine walls, potentially weakening their structural integrity and increasing the likelihood of a moraine breach (Sattar *et al* 2025, Saha *et al* 2025). This illustrates the critical role of calving events in influencing the lake's stability and the associated risk of GLOF. Similar studies of high-risk glacial lakes in the Bhutan Himalaya (Rinzin *et al* 2023), Imja and Tsho Rolpa lakes in the Nepal Himalaya (Watanabe *et al* 2009, Shrestha *et al* 2010) have documented glacier calving as a significant process influencing proglacial lake stability. These studies provide evidence that calving-induced wave propagation can exert considerable pressure on the moraine walls, leading to potential destabilization and increased risk of moraine failure. If a glacier is within 1.5 km of a lake, the possibility of calving or avalanches into the lake increases significantly (Campbell *et al* 2012), which in the case of SLL is less than 100 m from the SLG terminus. Even minor ice avalanches from hanging or calving glaciers can represent a serious potential for a secondary hazard when they collapse into moraine-dammed glacial lakes (Richardson and Reynolds 2000). The gradual increase in SLL volume as a result of accelerated glacier melt and calving over the past years (figures 1 and 2) has reduced the glacier stability, which are possible drivers to the calving and rapid retreat that occurred between 27 September and 6 October 2023.

4.2.2. Moraine instability and change in permafrost occurrence

Historical imagery since 1962 (figure S3) reveal discontinuities in the north lateral moraine, coupled with a stream flowing along this moraine wall had previously suggested potential GLOF hazard (Sharma *et al* 2018). The moraine weakening can be attributed to several factors. Thinning and retreating SLG likely reduced the support provided by ice to lateral moraines, leading to glacial debuttressing and weakening slope stability (Deline *et al* 2021, Sattar *et al* 2025), potentially leading to the moraine failures. Discontinuous moraines are particularly prone to failure, especially under the increased pressure from an expanding glacial lake. In SLL, the lateral moraine was discontinuous since the Lhonak glacier is detached from the SLG (figures 3(a) and S3). Also, historical percolation of rainwater (e.g. Yu *et al* 2024) and snowmelt has likely caused progressive internal erosion and destabilization of the moraine, as documented in previous studies that show how hydrological processes, including seepage and internal ice melt, weaken moraine stability over time (Richardson and Reynolds 2000, Harrison *et al* 2018). This is particularly critical in areas where moraines contain ice cores or are composed of unconsolidated materials, which become susceptible to collapse under the weight of the impounded lake water (Westoby *et al* 2014, Fischer *et al* 2015). In the case of SLL, post-GLOF imagery acquired on 6 October indicate the presence of dead ice core remains towards the terminal moraine breached areas (figure 1(d)), similar to observations from other moraine-dammed glacial lakes (e.g. Clague and Evans 2000, Harrison *et al* 2018, Medeu *et al* 2022).

Our study shows the high probability fraction of permafrost near SLG and surrounding areas of SLL, based on the derived products from Gruber (2012) and Obu *et al* (2019), with a higher fraction in the Obu *et al* (2019) dataset. The discrepancy between the two products in this region is likely due to the difference in the temperature data. Gruber (2012) used the Mean Annual Air Temperature (MAAT), while Obu *et al* (2019) used Mean Annual Ground Temperature (MAGT). The latter model is validated using the *in situ* borehole measurements data and with a higher accuracy in mountains. However, we still do not have any regional model to confirm the accuracy of the permafrost locations in the Himalaya from these two products. The 2016 GLOF at Imja Lake in Nepal highlighted how increased lake levels and weakened moraine stability due to permafrost thawing led to an outburst flood (Kroczek and Vilimek 2021). Thawing permafrost at high slopes due to increased temperature destabilised the ground and induces mass wasting processes, which may displace large volumes of debris into the moraine or directly into the lake, triggering a cascading event that can lead to moraine failure, induce landslides, contributing to slope instability and mass wasting and subsequent GLOFs (Huggel *et al* 2004, Gruber and Haeberli 2007, Haeberli *et al* 2010, Worni *et al* 2012). These processes, in combination with intermittent rainfall and seasonal snowmelt, and ground destabilisation, contributed to the weakened state of the lateral moraine along the flow path from NLG to SLL. This weakening has likely resulted in the moraine's instability, amplifying the risk of GLOFs due to glacier calving, wave generation, and moraine breach (Huggel *et al* 2004). The cascading events observed, where mass wasting temporarily elevates the lake level, triggering calving and further increasing pressure on the terminal moraine are well-documented mechanisms in GLOF triggering processes (Worni *et al* 2014).

4.2.3. Rainfall and local geomorphology

In comparison with other significant GLOFs in the Indian Himalaya, the Kedarnath disaster is the only high-fatality event known that involved heavy rainfall and caused the failure of a pro/moraine-dammed lake. This

was due to extreme rainfall of 390 mm over a week, which caused the moraines around the Chorabari Lake to collapse (e.g. Allen *et al* 2016). Also, the 2010 GLOF event in the Chujin Lake illustrates how extreme weather events and fluctuating lake levels led to catastrophic moraine-dam breaches (Liu *et al* 2014).

In our study, the GPM based maximum daily rainfall in and around SLL was around 15 mm during September, before the GLOF event, ruling out any extreme rainfall as the main trigger for the event (figure 4). However, local weather stations across Sikkim state recorded 101 mm of rainfall during the first 5 days of October 2023 and reached 115–205 mm of rainfall on 4 October 2023 (~5 times above the seasonal average between 2018 and 2022), coinciding with the SLL GLOF event (Yu *et al* 2024, Zhang *et al* 2024). Although these studies have not indicated the location/source of these rainfall data, we observe a large discrepancy with corresponding daily station rainfall and considerably underestimated monthly rainfall patterns. This indicates that the GPM resolution of 10 km^2 is perhaps not able to capture the local scale modifications of the climate by vegetation and topography (Zellweger *et al* 2019). Lu *et al* (2021) reported underestimated precipitation in areas with solid precipitation for IMERG data, particularly in high elevation zones. Therefore, even if any extreme precipitation event(s) has occurred immediately before the GLOF at a considerably high elevation of 5200 m, GPM IMERG data may not have been able to capture it. Notably, though PlanetScope data is available at a daily temporal resolution, the lake was completely cloud covered from 30 September and the first cloud free data was available only on 6 October. This indicates the possibility of rainfall during this cloudy period, but it is difficult to guess how extreme the rainfall would have been.

The average annual rainfall for Chungthang Station is considerable, around 2500 mm. As rainfall percolates through the snow and glacial ice, the entire snow volume becomes saturated, creating wet snow and/or slush, increasing the weight of the snow (Gubler and Bader 1989). This will cause the snow meltwater to flow across/through the glacier terminus/volume (bed) and into the lake, especially where the slope exceeded 10° (Richarson and Reynolds 2000). Moreover, in many cases, a snowpack does not respond to artificial control measures before it starts to rain. However, it will often avalanche naturally soon after the rain begins (Conway and Raymond 1993). Also, a high rate of basal shear strain can make a snowpack unstable (Gubler and Bader 1989). Additionally, the slope's normal force causes the snow slab to bend, which can further contribute to instability. As the flow moves downslope, it potentially entrains a large amount of snow through an actively eroding snow avalanche channel and over the steep medial moraine at the eastern margin and proglacial area of the glacier. These processes suggest that even if extreme rainfall had not immediately preceded the GLOF event based on the station-based and GPM rainfall observations, any substantial annual rainfall or extended periods of heavy rainfall, as reported by Zhang *et al* (2024) and Yu *et al* (2024) would have played a crucial role in progressively weakening the glacier's stability over time.

4.2.4. Comparison with recent studies on the South Lhonak Lake GLOF event

Recent studies (Kaushik *et al* 2024, Singh *et al* 2025, Yu *et al* 2024, Zhang *et al* 2024, Sattar *et al* 2025, Saha *et al* 2025) of the 2023 SLL GLOF event utilized post-GLOF field observations, seismic interpretation, and hydrodynamic or terrain modeling. These studies identified moraine collapse, landslide-generated waves, and heavy rainfall as the primary triggers for the GLOF, as well as evaluated the downstream impact of the flood. However, they are limited in temporal coverage, between 5–20 years, and primarily address immediate hazard mechanisms. In comparison, our study complements these studies, however, distinguishes itself through a six-decade-long (1962–2023) geomorphic reconstruction of the SLG–SLL system using high-resolution stereo, optical and SAR imagery from 10 different satellite missions and DEM differencing techniques. In contrast to other works, our study quantifies long-term glacier thinning trends (up to –0.87 m $year^{-1}$ in recent years), a 12-fold lake expansion, and identify seven SLG calving events between 2017 and 2023; including a significant SLG retreat of 49.6 $\pm$ 7.1 m just 10 days prior to the GLOF event. This rapid calving event, combined with historical calving events, intermittent rainfall prior to GLOF and the destabilization of lateral moraines, is proposed here as a combination of primary triggers of the moraine failure; a set of mechanisms not explicitly quantified in previous studies.

Furthermore, we integrate historical evidence of moraine evolution and changes, along with the occurrence of permafrost into our interpretation of moraine instability, thus providing a detailed picture of the GLOF preconditioning controls. Although, studies by Zhang *et al* (2024) and Yu *et al* (2024) document slope-based or InSAR evidence of moraine movement, these studies neglect the importance of long-term moraine changes and SLG calving quantification that we have presented. Our results, therefore, complement existing hazard and modeling studies and go beyond by investigating the cumulative role of rapid and historical SLG retreat, thinning, and moraine debuttressing in shaping SLL's instability.

5. Conclusions

In this study, we quantify the geomorphological evolution of the South Lhonak Lake from 1962 to 2023, driven by the retreat of the South Lhonak Glacier, its calving history, and the geomorphic changes that culminated in the 2023 South Lhonak GLOF event, using historical, multi-source satellite data. The glacier's retreat and calving history and processes have contributed significantly to the lake's expansion, while the evolving geomorphology around the lake provided crucial precursors to the triggering of the GLOF event. The glacier system has undergone significant changes during this time, with a 12-fold enlargement of the moraine-dammed SLL. Our findings indicate strong changes in moraine dam stability, with high-resolution DEM data indicating significant topographic changes. Optical and SAR satellite-observed rapid glacier retreat of >49 m before the GLOF event, occurrence of 7 major glacier calving events since 2017, coupled with intermittent rainfall, and breach of lateral and terminal moraine walls likely triggered the GLOF event on 6 October 2023. Although rainfall did not appear to be a major trigger in this instance, the interaction between rapid glacial melt from the glacier complex, suspected potential thaw and subsidence of permafrost cover above the moraines, and historically observed unstable moraine walls present a growing challenge for managing the risks posed by GLOFs in the region. There are no methods available in the literature which differentiate the ice cored moraines and permafrost in the deglaciated areas, which may have been misidentified as permafrost in the regions around SLL. This can be improved by collecting the ice core on moraine and active layer thickness of the permafrost from the field investigation. The absence of extensive field observations (except for post-GLOF measurements reported by Sattar *et al* (2025) limits the validation of remote sensing and modelling results. Future efforts should integrate remote sensing, modelling, and extensive field observations to enhance the accuracy and reliability of GLOF predictions.

Acknowledgments

The authors declare that they have no competing interests. We acknowledge the research funding (Grant no. CRG/2021/002450) received from Anusandhan National Research Foundation (ANRF), Department of Science and Technology (DST), India. We are grateful to the satellite data providers: USGS for Landsat, and JPL/NASA and METI for ASTER, ESA for Sentinel-1 and 2, National Remote Sensing Centre (NRSC), India for Cartosat-1. We are grateful to CNES/Airbus DS for the provision of the Pléiades satellite data within the ISIS program and the Pléiades Glacier Observatory facilitated by Etienne Berthier (LEGOS) and Delphine Fontannaz (CNES). We are also thankful to the India Meteorological Department (IMD), Regional Meteorological Center (RMC), Kolkata for providing weather station data.

Data availability statement

All data that support the findings of this study are included within the article (and any supplementary files).

Author contributions

Remya S N 0000-0001-8960-7033
Conceptualization (lead), Formal analysis (equal), Investigation (lead), Methodology (lead), Project administration (equal), Writing – original draft (equal), Writing – review & editing (equal)

Vishnu Nandan 0000-0002-5133-2676
Conceptualization (equal), Data curation (supporting), Formal analysis (equal), Funding acquisition (lead), Investigation (equal), Methodology (equal), Visualization (equal), Writing – original draft (equal), Writing – review & editing (lead)

Atanu Bhattacharya 0000-0001-7449-3897
Data curation (equal), Methodology (equal), Visualization (equal), Writing – review & editing (equal), Writing – original draft (equal)

Pradeep Srinivasalu 0000-0001-6404-8845
Data curation (equal), Software (equal), Visualization (equal)

Kriti Mukherjee 0000-0002-2290-2676
Data curation (equal), Investigation (supporting), Software (equal), Visualization (equal), Writing – original draft (equal)

Babu Govindha Raj 0000-0003-1311-7710
Conceptualization (supporting), Investigation (equal), Methodology (supporting), Writing – original draft (supporting)

John Yackel
Writing – original draft (equal), Writing – review & editing (supporting), Investigation (supporting)

Tobias Bolch
Formal analysis (supporting), Writing – original draft (supporting), Writing – review & editing (supporting), Supervision (lead)

References

Ahmed R, Wani G F, Ahmad S T, Sahana M, Singh H and Ahmed P 2021 A review of glacial lake expansion and associated glacial lake outburst floods in the Himalayan region *Earth Syst. Environ.* **5** 695–708
Allen S K, Rastner P, Arora M, Huggel C and Stoffel M 2016 Lake outburst and debris flow disaster at Kedarnath, June 2013: hydrometeorological triggering and topographic predisposition *Landslides* **13** 1479–91
Allen S K, Sattar A, King O, Zhang G, Bhattacharya A, Yao T and Bolch T 2022 Glacial lake outburst flood hazard under current and future conditions: worst-case scenarios in a transboundary Himalayan basin *Nat. Hazards Earth Syst. Sci.* **22** 3765–85
Basnett S, Kulkarni A V and Bolch T 2013 The influence of debris cover and glacial lakes on the recession of glaciers in Sikkim Himalaya, India *J. Glaciol.* **59** 1035–46
Bhambri R, Bolch T and Chaujar R K 2012 Frontal recession of Gangotri Glacier, Garhwal Himalayas, from 1965 to 2006, measured through high-resolution remote sensing data *Curr. Sci.* **102** 489–94 (https://currentscience.ac.in/Volumes/102/03/0489.pdf)
Bolch T, Yao T, Kang S, Buchroithner M F, Scherer D, Maussion F, Huintjes E and Schneider C 2010 A glacier inventory for the western Nyainqentanglha Range and the Nam Co Basin, Tibet, and glacier changes 1976–2009 *The Cryosphere* **4** 419–33
Brun F, Berthier E, Wagnon P, Kääb A and Treichler D 2017 A spatially resolved estimate of High Mountain Asia glacier mass balances from 2000 to 2016 *Nat. Geosci.* **10** 668–73
Campbell S, Kreutz K, Osterberg E, Arcone S, Wake C, Introne D and Winski D 2012 Melt regimes, stratigraphy, flow dynamics and glaciochemistry of three glaciers in the Alaska Range *J. Glaciol.* **58** 99–109
Carrivick J L and Tweed F S 2016 A global assessment of the societal impacts of glacier outburst floods *Global Planet. Change* **144** 1–16
Clague J J and Evans S G 2000 A review of catastrophic drainage of moraine-dammed lakes in British Columbia *Quat. Sci. Rev.* **19** 1763–83
Conway H and Raymond C F 1993 Snow stability during rain *J. Glaciol.* **39** 635–42
Deline P, Gruber S, Amann F, Bodin X, Delaloye R, Failletaz J and Weber S 2021 Ice loss from glaciers and permafrost and related slope instability in high-mountain regions *In Snow and Ice-Related Hazards, Risks, and Disasters* (Elsevier) pp 501–40 (10.1016/B978-0-12-817129-5.00015-9)
Emmer A 2018 GLOFs in the WOS: bibliometrics, geographies and global trends of research on glacial lake outburst floods (Web of Science, 1979–2016) *Nat. Hazards Earth Syst. Sci.* **18** 813–27
Falaschi D, Bhattacharya A, Guillet G, Huang L, King O, Mukherjee K, Rastner P, Yao T and Bolch T 2023 Annual to seasonal glacier mass balance in High Mountain Asia derived from Pléiades stereo images: examples from the Pamir and the Tibetan Plateau *Cryosphere* **17** 5435–58
Fischer M, Huss M and Hoelzle M 2015 Surface elevation and mass changes of all Swiss glaciers 1980–2010 *Cryosphere* **9** 525–40
Förstner M A and Gülch E 1987 A fast operator for detection and precise location of distinct points, corners and centres of circular features *Proceedings of the ISPRS Intercommission Confe-rence on Fast Processing of Phonogrammic Data (Interlaken, 2-4 June 1987)* pp 281–305 (https://cseweb.ucsd.edu/classes/sp02/cse252/foerstner/foerstner.pdf)
Ghuffar S, King O, Guillet G, Rupnik E and Bolch T 2023 Brief communication: Glacier mapping and change estimation using very high-resolution declassified Hexagon KH-9 panoramic stereo imagery (1971–1984) *Cryosphere* **17** 1299–306
Goerlich F, Bolch T, Mukherjee K and Pieczonka T 2017 Glacier mass loss during the 1960s and 1970s in the Ak-Shirak range (Kyrgyzstan) from multiple stereoscopic Corona and Hexagon imagery *Remote Sens.* **9** 275
Granshaw F D and Fountain A G 2006 Glacier change (1958–1998) in the northCascades national park complex, Washington, USA *J. Glaciol.* **52** 251–6
Gruber S 2012 Derivation and analysis of a high-resolution estimate of global permafrost zonation *The Cryosphere* **6** 221–33
Gruber S and Haeberli W 2007 Permafrost in steep bedrock slopes and its temperature-related destabilization following climate change *J. Geophys. Res.:Earth Surf.* **112** 405–17
Gubler H and Bader H P 1989 A model of initial failure in slab-avalanche release *Ann. Glaciol.* **13** 90–5
Haeberli W, Noetzli J, Arenson L, Delaloye R, Gärtner-Roer I, Gruber S and Phillips M 2010 Mountain permafrost: development and challenges of a young research field *J. Glaciol.* **56** 1043–58
Haeberli W, Schaub Y and Huggel C 2017 Increasing risks related to landslides from degrading permafrost into new lakes in de-glaciating mountain ranges *Geomorphology* **293** 405–17
Hall D K, Bayr K J, Schöner W, Bindschadler R A and Chien J Y 2003 Consideration of the errors inherent in mapping historical glacier positions in Austria from the ground and space (1893–2001) *Remote Sens. Environ.* **86** 566–77
Harrison S *et al* 2018 Climate change and the global pattern of moraine-dammed glacial lake outburst floods *Cryosphere* **12** 1195–209
Harrison S, Kargel J S, Huggel C, Reynolds J, Shugar D H, Betts R A and Vilímek V 2018 Climate change and the global pattern of moraine-dammed glacial lake outburst floods *Cryosphere* **12** 1195–209
Huffman G J, Bolvin D T, Braithwaite D, Hsu K L, Joyce R J, Kidd C and Xie P 2020 Integrated multi-satellite retrievals for the global precipitation measurement (GPM) mission (IMERG) *Satellite Precipitation Measurement* **1** 343–53

Huggel C, Haeberli W, Kääb A, Bieri D and Richardson S 2004 An assessment procedure for glacial hazards in the Swiss Alps *Can. Geotech. J.* **41** 1068–83
Huss M 2013 Density assumptions for converting geodetic glacier volume change to mass change *Cryosphere* **7** 877–87
Immerzeel W W, Lutz A F, Andrade M, Bahl A, Biemans H, Bolch T and Baillie J E M 2020 Importance and vulnerability of the world's water towers *Nature* **577** 364–9
Kaushik S, Rafiq M, Dharpure J K, Howat I, Moortgat J, Joshi P K, Singh T and Dietz A J 2024 Increasing risk of glacial lake outburst flood in Sikkim, Eastern Himalaya under climate warming *Remote Sensing Applications: Society and Environment* **36** 101286
Kroczek T and Vilimek V 2021 Rockfall/rockslide hazard, lake expansion and dead-ice melting assessment: Lake Imja, Nepal *Understanding and Reducing Landslide Disaster Risk. WLF 2020* (*ICL Contribution to Landslide Disaster Risk Reduction*) ed V Vilímek *et al* (Springer) pp 103–10
Liu J J, Cheng Z L and Su P C 2014 The relationship between air temperature fluctuation and Glacial Lake Outburst Floods in Tibet, China *Quat. Int.* **321** 78–87
Lu C, Ye J, Fang G, Huang X and Yan M 2021 Assessment of GPM IMERG satellite precipitation estimation under complex climatic and topographic conditions *Atmosphere* **12** 780
McNabb R, Nuth C, Kääb A and Girod L 2019 Sensitivity of glacier volume change estimation to DEM void interpolation *Cryosphere* **13** 895–910
Medeu A R, Popov N V, Blagovechshenskiy V P, Askarova M A, Medeu A A, Ranova S U and Bolch T 2022 Moraine-dammed glacial lakes and threat of glacial debris flows in South-East Kazakhstan *Earth Sci. Rev.* **229** 103999
Nuth C and Kääb A 2011 Co-registration and bias corrections of satellite elevation data sets for quantifying glacier thickness change *Cryosphere* **5** 271–90
Obu J *et al* 2019 Northern Hemisphere permafrost map based on TTOP modelling for 2000–2016 at 1 km2scale *Earth-Sci. Rev.* **193** 299–316
Pieczonka T and Bolch T 2015 Region-wide glacier mass budgets and area changes for the Central Tien Shan between ~1975 and 1999 using Hexagon KH-9 imagery *Glob. Planet. Change.* **128** 1–13
Raj K B G, Remya S N and Kumar K V 2013 Remote sensing-based hazard assessment of glacial lakes in Sikkim Himalaya *Curr. Sci.* **104** 359–64 (https://currentscience.ac.in/Volumes/104/03/0359.pdf)
Remya S N, Kulkarni A V, Pradeep S and Shrestha D G 2019 Volume estimation of existing and potential glacier lakes, Sikkim Himalaya, India *Curr. Sci.* **116** 620–7 (https://jstor.org/stable/27137905)
Remya S N, Syed T H, Kulkarni A V, Nainwal H C and Mishra A 2024 Observing changes in the present and paleo-glacial extents of major glaciers in the Alaknanda Basin of Central Himalaya *Geomorphology* **461** 109287
Richardson S D and Reynolds J M 2000 An overview of glacial hazards in the Himalayas *Quat. Int.* **65–66** 31–47
Rinzin S, Zhang G, Sattar A, Wangchuk S, Allen S K, Dunning S and Peng M 2023 GLOF hazard, exposure, vulnerability, and risk assessment of potentially dangerous glacial lakes in the Bhutan Himalaya *J. Hydrol.* **619** 129311
Saha S, Bera B, Sengupta D, Mukhopadhyay U, Ghosh D, Tamang L, Bhattacharjee S and Sengupta N 2025 Multiple drivers of the recent South Lhonak glacial lake outburstflood in Sikkim Himalaya and its aftermath on Teesta River Valley *Geosystems and Geoenvironment* **4** 100375
Sattar A, Cook K L, Rai S K, Berthier E, Allen S, Rinzin S and Bhat S Y 2025 The Sikkim flood of October 2023: Drivers, causes and impacts of a multihazard cascade *Science* **387** eads2659
Sattar A, Goswami A, Kulkarni A V, Emmer A, Haritashya U K, Allen S and Huggel C 2021 Future glacial lake outburst flood (GLOF) hazard of the South Lhonak Lake, Sikkim Himalaya *Geomorphology* **388** 107783
Sharma R K, Pradhan P, Sharma N P and Shrestha D G 2018 Remote sensing and *in situ*-based assessment of rapidly growing South Lhonak glacial lake in eastern Himalaya, India *Nat. Hazards* **93** 393–409
Shrestha A B, Eriksson M, Mool P, Ghimire P, Mishra B and Khanal N R 2010 Glacial lake outburst flood risk assessment of Sun Koshi basin, Nepal *Geomatics, Natural Hazards and Risk* **1** 157–69
Singh A, Anand V, Durga Rao K H V and Chauhan P 2025 Unveiling the catastrophic landslide-induced flash flood in Teesta River, Sikkim: insight from South Lhonak Glacial Lake *Landslides* **22** 837–55
Sohn H G, Kim G H and Yom J H 2004 Mathematical modelling of historical reconnaissance CORONA KH-4B imagery *The Photogrammetric Record* **19** 51–66
Staines K E and Carrivick J L 2015 Geomorphological impact and morphodynamic effects on flow conveyance of the 1999 jökulhlaup at sólheimajökull, Iceland *Earth Surf. Processes Landforms* **40** 1401–16
Taylor C, Robinson T R, Dunning S, Rachel Carr J and Westoby M 2023 Glacial lakeoutburst floods threaten millions globally *Nat. Commun.* **14** 487
Watanabe T, Lamsal D and Ives J D 2009 Evaluating the growth characteristics of a glacial lake and its degree of danger of outburst flooding: Imja Glacier, Khumbu Himal, Nepal *Norsk Geografisk Tidsskrift-Norwegian Journal of Geography* **63** 255–67
Westoby M J, Glasser N F, Brasington J, Hambrey M J, Quincey D J and Reynolds J M 2014 Modelling outburst floods from moraine-dammed glacial lakes *Earth Sci. Rev.* **134** 137–59
Worni R, Huggel C, Clague J J, Schaub Y and Stoffel M 2014 Coupling glacial lake impact, dam breach, and flood processes: a modeling perspective *Geomorphology* **224** 161–76
Worni R, Stoffel M, Huggel C, Volz C, Casteller A and Luckman B 2012 Analysis and dynamic modeling of a moraine failure and glacier lake outburst flood at Ventisquero Negro, Patagonian Andes (Argentina) *J. Hydrol.* **444** 134–45
Yu Y, Li B, Li Y and Jiang W 2024 Retrospective analysis of glacial lake outburst flood (glof) using ai earth insar and optical images: a case study of south lhonak lake, sikkim *Remote Sens.* **16** 2307
Zellweger F, Coomes D, Lenoir J, Depauw L, Maes S L, Wulf M and De Frenne P 2019 Seasonal drivers of understorey temperature buffering in temperate deciduous forests across Europe *Glob. Ecol. Biogeogr.* **28** 1774–86
Zemp M, Huss M, Thibert E, Eckert N, McNabb R, Huber J and Cogley J G 2019 Global glacier mass changes and their contributions to sea-level rise from 1961 to 2016 *Nature* **568** 382–6
Zhang T, Wang W and An B 2024 Heterogeneous changes in global glacial lakes undercoupled climate warming and glacier thinning *Communications Earth & Environment* **5** 374
Zhang T, Wang W, An B, Gao T and Yao T 2022 Ice thickness and morphological analysis reveal the future glacial lake distribution and formation probability in the Tibetan Plateau and its surroundings *Glob. Planet. Change* **216** 103923
Zheng G, Allen S K, Bao A, Ballesteros-Cánovas J A, Huss M, Zhang G and Stoffel M 2021 Increasing risk of glacial lake outburst floods from future Third Pole deglaciation *Nat. Clim. Change* **11** 411–7